Chapter 5
Measuring Infrasound from the Maritime Environment

Doug Grimmett, Randall Plate and Jason Goad

Abstract Worldwide infrasound coverage is obtained using fixed, land-based sensing networks. However, two-thirds of the earth's surface is composed of oceans, and while islands in the ocean already host sensing stations, no capability yet exists to monitor infrasound from sensors fielded directly in the maritime environment. Deployment in the maritime would greatly enhance the ability to monitor natural and anthropogenic sources of infrasound around the world through improved event detection, localization, and classification. The additional sensing may also facilitate improved knowledge of global atmospheric environmental conditions. The advantages and challenges of infrasound sensing in the maritime environment are described, as are potential host platforms for fielding them. Some technical challenges for this concept include sensor motion, wind noise, composing arrays of sensors and survivability in the ocean environment. An in-depth analysis of one of these, the negative impact of ocean heave on performance, is described along with a potential solution for its mitigation.

5.1 Introduction

A variety of natural and anthropogenic sources produce very-low-frequency acoustic waves that can be received hundreds to thousands of kilometers away. These acoustic waves are typically in the infrasound band, between 0.033 and 20 Hz, and below human hearing range. Land-based microbarometer sensors and networks have shown the capability of detecting infrasound signals originating from natural and anthropogenic sources. Natural sources of infrasound include earthquakes, meteors, volcanoes, tsunamis, auroras, and ocean swells (Christie and Campus 2010). Among anthropogenic sources are atmospheric and underground nuclear explosions.

D. Grimmett (✉) · R. Plate
SPAWAR Systems Center Pacific, San Diego, USA
e-mail: grimmett@spawar.navy.mil

J. Goad
Florida Atlantic University, Boca Raton, USA

A. Le Pichon et al. (eds.), *Infrasound Monitoring for Atmospheric Studies*,
https://doi.org/10.1007/978-3-319-75140-5_5

Because of their low frequency, infrasound waves experience little attenuation, and can, therefore, propagate to, and be detectable from, very long distances. Although the signals are inaudible, they may be detected using advanced infrasound sensing technology at ranges of 100s–1000s of kilometers (Marty 2019; Mialle et al. 2019).

The Comprehensive Nuclear Test Ban Treaty Organization (CTBTO) operates a worldwide network of 60 infrasound monitoring stations (Christie and Campus 2010), as shown in Fig. 5.1. The primary purpose is to detect nuclear test explosions, and approximately 85% of the network is currently operational (Marty 2019). The USArray Transportable Array (TA) is a wide area network of 400 seismic sensors with about 70 km spacing, deployed and redeployed over various regions of the United States since 2007 (the current deployment region is in Alaska). Most of these stations also include a single infrasound sensor, in addition to the primary seismic sensor, to monitor atmospheric signals (Meltzer 1999). These, and other national and international land-based infrasound sensors, sensor arrays, and networks, are located across the globe and are capable of detecting natural and anthropogenic sources of infrasound occurring at great distances (Nief et al. 2019).

Wide infrasound coverage is obtained using such fixed, land-based sensing networks. However, two-thirds of the earth's surface is composed of oceans, and while islands in the ocean host sensing stations, no capability yet exists to monitor infrasound from sensors fielded directly in the maritime environment. In this chapter, we investigate the potential of such maritime fielding of microbarometer sensors on boats, buoys, or unmanned surface vehicles (USVs). The potential advantages of such a maritime infrasound capability, and the technical challenges to be overcome, are discussed. One particular problem to be overcome is the effect of ocean heave on sensor performance. Vertical motion, such as that produced by ocean heave, induces interfering pressure fluctuations on the sensor which may obscure the infrasound signals-of-interest. An approach to overcome this interference is described using an external heave measurement and an adaptive noise cancellation algorithm (Grimmett et al. 2016).

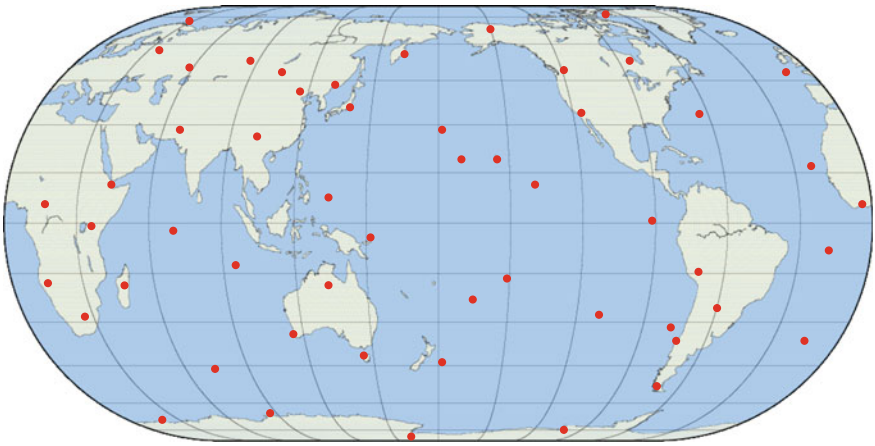

Fig. 5.1 The locations of CTBTO infrasound monitoring stations worldwide

In addition to maritime infrasound, other nontraditional, non-land-based infrasound collection environments are being explored, such as sensors being hosted by balloons in the atmosphere (Bowman et al. 2019).

5.2 Advantages of Infrasound Measurements from the Maritime Environment

The challenges of developing a working maritime infrasound sensing capability may be significant; however, if overcome, it offers great potential for improvements in infrasound signal detection, localization, classification, and environmental assessment.

5.2.1 Detection

To achieve global worldwide coverage, about 15 of the currently operating CTBTO infrasound monitoring stations are located on remote islands, amidst vast ocean expanse, thousands of miles from the earth's continental land masses. For example, CTBTO stations at Midway (IS58) and Tahiti (IS24) are located in the middle of the vast Pacific Ocean, Kerguelen (IS23) is in a remote area of the South Indian Ocean, and Tristan da Cunha (IS49) is in the middle of the South Atlantic Ocean. Even though these remotely located island stations may be thousands of kilometers from neighboring stations, they are a key adjunct to the CTBTO continental-based stations; without them, the network would be unable to provide adequate global infrasound detection coverage (Green and Bowers 2010; Le Pichon et al. 2019).

Outside the CTBTO network, national or other infrasound networks may be very limited in their coverage, being constrained by available land locations and perhaps national borders. The placement of infrasound sensors in the oceans has the potential to provide an expansive, new, remote environment from which infrasound signal detection can be made to supplement the coverage obtained with land-based networks. Placement of sensors in ocean locations may offer coverage where it does not exist, or when current land-based monitoring coverage is less reliable due to fluctuating environmental conditions. Gaps in detection coverage may be filled with appropriate placement and operations from the technology deployed directly in the oceans.

Performance of infrasound sensor detection coverage is a function of many variables, but foremost is the location of the sensor(s) and the prevailing environmental conditions. The atmospheric conditions between the infrasound signal-of-interest and the sensor will largely determine whether there will be a viable propagation path connecting them. The propagation is a function of the sound velocity profile, which is mainly dependent on temperature gradients and wind, and can either result in connected stratospheric, thermospheric, or surface-ducted paths,

or in shadow zones where significant energy does not arrive (de Groot-Hedlin et al. 2010; Waxler and Assink 2019). The infrasound signal frequency will determine how much attenuation it is subjected to before arriving at a sensor. The presence of gravity waves can further complicate and modify the expected propagation conditions (de Groot-Hedlin et al. 2010). Further, these environmental factors vary over time, which, in turn, affects the performance at the infrasound sensor. Perhaps the most obvious example of this is the seasonal effect of the stratospheric winds (de Groot-Hedlin et al. 2010; Le Pichon et al. 2012; Ceranna et al. 2019). Zonal winds shift from easterly in summer, to westerly in winter; noting that the Northern hemisphere summer occurs during the Southern hemisphere winter. (de Groot-Hedlin et al. 2010). Good infrasound propagation is achieved when traveling downwind; therefore, a station's best zonal coverage performance area will switch east to west and west to east with the seasons, twice a year. Maritime infrasound sensors may be situated to augment existing land-based coverage in desired directions during the "difficult" season. For example, a source of infrasound originating on a continent's east coast in the northern hemisphere may be detected by a further inland, land-based monitoring station to the west during summer. However, during winter the favorable propagation direction will be to the east, where only ocean, not land, is available to optimally position a receiving infrasound station. Further, it is well known that infrasound background noise levels are diurnal: higher levels are seen during daytime than nighttime (de Groot-Hedlin et al. 2010). A greater spatial distribution of sensors may yield better performance by having nodes favorably positioned such that they are in a time of lower diurnal-induced background noise level at the time of signal reception. Additionally, some sources of infrasound have very directional propagation properties, like the shock waves associated with meteors and bolides traveling at supersonic/hypersonic speeds. In such cases, the direction of acoustic propagation is nearly perpendicular to the line-of-flight, so only sensors situated properly relative to the trajectory and with a good propagation path are likely to receive the infrasound signal (Pilger et al. 2015). The more sensors that are available to be distributed geographically, the more diverse detection opportunities are presented; robustness to infrasound signal detection and coverage of infrasound source locations is therefore improved.

5.2.2 Event Localization and Classification

Infrasound event detection is merely a starting point. Data and information fusion between multiple infrasound stations provide valuable additional information. When multiple stations detect an event, the joint information may be used to provide a localization estimate of the detected signals' common source. Processing of a single infrasound array can provide an estimate of the arriving signal's back azimuth, but it does not provide the range to the event (Cansi 1995). When multiple arrays observe the same infrasound event, their respective back-azimuth estimates may be combined through a cross-fixing process to provide a localization estimate

(Bratt and Bache 1988; Mialle et al. 2019). The more arrays that are combined, and the more that these arrays are located in geometrically advantageous (diverse) ways (i.e., with orthogonal look directions to the event), the better the localization estimate's accuracy. Even if the infrasound stations are only composed of a single sensor (as in the USArray's Transportable Array) rather than an array, and are unable on their own to determine a back azimuth, correlation methods have shown that events can be localized with a sparse network of nondirectional sensors (De Groot-Hedlin and Hedlin 2015; Vergoz et al. 2019; de Groot-Hedlin and Hedlin 2019). Further, if the infrasound source is moving, as in the case of a meteor/bolide, a network of sensors is better able to track its trajectory through time. In addition to localization and tracking benefits, being able to correlate events among multiple sensors provides increased detection confidence and additional data to better classify the type of infrasound event, as well as derive quantities of interest about the source event which produced it. In some cases, reduction in false alarm rate can be achieved by requiring a minimum number of correlated detections from different stations. Better infrasound coverage in the oceans could provide a more regular grid, and would avoid network configuration asymmetries that are constrained by land-only installations. It is clear then that adding additional sensors to a sensing network is advantageous, and, therefore, introducing sensors into the maritime environment offers to improve infrasound event localization, tracking, and classification. This is done by providing greater geographic distribution and geometric diversity that would not be possible when limited to land-based sites.

5.2.3 Environmental Assessment

Infrasound propagation is subject to a variety of atmospheric conditions. It is essential to understand the effects of the environment in order to understand infrasound monitoring performance. Signal detection will depend on propagation paths and their losses, and the environment may also significantly modify the source signal along its propagation path to a sensor (e.g., it may spread the signal in time, etc.). Modeling infrasound depends on environmental descriptions, which are not always known well enough to produce accurate results (Drob 2019; Waxler and Assink 2019; Chunchuzov and Kulichkov 2019). Often the environmental descriptions are averages over large areas, or they are historical instead of for the current time. With infrasound sensors operating in different locations (including vast oceanic areas), inversion techniques (Drob et al. 2010; Assink et al. 2019) can be used to obtain better estimates and understanding of the atmospheric effects and conditions worldwide which impact infrasound performance. Having sensors in the maritime environment will provide richer data collection opportunities to support scientific studies of the atmosphere and provide environmental assessments for operational systems.

5.3 Challenges of Infrasound Measurements from the Maritime Environment

The sensor most often employed to measure infrasound is the microbarometer, which provides very accurate measurements of acoustic signals with very low frequency. Microbarometers are typically designed for outdoor use on land, where they can maintain performance during exposure to the elements. Land-based monitoring sites are normally composed of multiple (up to 10) sensors spaced from a few hundred meters to a few kilometers apart, each with a wind filtering system, forming an array. The stations include data acquisition and communication technology and the required electrical power for operations. The systems are calibrated appropriately for their installed locations. There will be significant challenges to fielding microbarometers in a maritime environment, compared to a land-based site.

5.3.1 Survivability

The maritime environment is a much harsher operating environment than most land sites. Exposure to extremes in weather and the effects of water, salt, wind, and humidity require significant efforts in ocean engineering to ensure system survivability, proper sensor operations, and to ensure a persistent operational capability. Waterproofing and weatherproofing of the system components will be essential. The sensor must be open to the atmosphere, but at the same time prevent water ingress, requiring some form of water shielding.

5.3.2 Sensor Motion

Maritime deployment will expose the sensor(s) to motion effects, since the hosting platform is likely to move with ocean swell/waves of a rough ocean surface. The sensor may experience motion along six degrees of freedom: surge, sway, yaw, pitch, roll, and heave. The most significantly impacting of these will be the heave motion, as even small changes in altitude will induce a change in the ambient atmospheric pressure. Microbarometer sensors will measure the pressure changes due to altitude changes, which look like an infrasound signal; in fact, it acts as an interference signal against which infrasound signals must be detected. Of all the technical challenges discussed here, this particular challenge has been addressed and will be discussed in more detail later.

In addition, some microbarometers are more sensitive to accelerations that are not necessarily accompanied by appreciable displacement than others. At this stage of investigation, it is unclear how different the acceleration effects on the sensor will be between land and maritime deployment. Should acceleration effects prove a significant degrading interference effect or performance-limiting factor, seismically decoupled or insensitive microbarometers may be preferred for maritime deployments.

5.3.3 Wind

Wind is the main contributor to the infrasound sensor's noise background level. Maritime environments are characteristically windy, and maritime deployment schemes will, therefore, require additional mitigation or compensation methods to reduce the negative impact of the resulting noise. Some oceanic locations and seasons will be exposed to lower winds than others and may be better suited for infrasound sensor deployment. During times of high seas and high winds, sensor performance may be compromised until calmer weather develops. Possible mitigation approaches are to develop suitable wind shrouds/filters/screens, or adaptive wind noise cancellation algorithms (Frazier 2014), tailored for use in a maritime environment.

5.3.4 Multi-element Arrays

To validate infrasound detections and determine their direction, arrays of infrasound sensors are usually employed. Since the sensor spacing for infrasound array elements is on the order of several hundreds of meters, maritime deployment will require multiple platforms. In some cases, they may be moving relative to one another, and sensor element positions must be tracked over time. Another implication is that this will require some telemetry to send the sensors' data to a fusion center for array processing.

Considering these challenges, the detection performance of a maritime infrasound monitoring system may be characterized as

$$SE = SL_{SOI} - TL + AG - [(N_{heave} - PG_{heave}) \oplus (N_{wind} - PG_{wind} - F_{wind}) \oplus N_{other}] - DT, \tag{5.1}$$

which is an equation for signal excess (SE) expressed in dB units, re 20 μPa. Signal excess is the amount of excess signal energy above the minimum required for the system to detect the infrasound signal-of-interest (SOI). Positive values indicate detectability, with higher values indicating stronger detections. SL_{SOI} is the sound pressure level of the SOI at its originating location, *TL* is the transmission loss (including the effects of spreading and absorption) along the propagation path from source to receiver, and *DT* is the detection threshold, i.e., how much signal-to-noise ratio is required before detections can be confidently called by the operator or automatic detection algorithm. For a given SOI, detection capability can be improved by locating the monitoring system such that a favorable propagation path connects the source and receiver, minimizing *TL*. *AG* is the processing or array gain achieved by combining multiple sensors of an array, either by correlation processes or beam forming. The background noise above which detection must be made is indicated by the power sum ($\oplus$) of the terms in brackets. The ocean heave interference, N_{heave}, may be reduced by implementation of an adaptive interference cancellation algorithm (described in detail later) providing a processing gain of PG_{heave}. The wind noise, N_{wind}, may be reduced/filtered by a physical screen or other system which provides a gain against the wind of F_{wind}. It may also be possible to reduce wind noise through adaptive processing approaches, providing a gain of PG_{wind}.

A processing approach for cancellation of the heave interference has been developed and will be described in more detail later. With a solution for heave interference available, wind mitigation remains a significant concern and challenge. Maritime wind noise in the infrasound band has yet to be studied in detail, and the amount of such noise that is mitigable is unknown. It is likely that infrasound wind noise is prevalent in the maritime environment and will thus be the detection-limiting term in the signal excess equation. Therefore, future efforts will investigate maritime wind noise and its mitigation.

5.4 Infrasound Sensor Hosts in the Maritime Environment

Infrasound sensors to be deployed in the maritime environment may be hosted on ships, ocean buoys, and unmanned surface vehicles (USVs). Figure 5.2 shows examples of various types of maritime infrasound sensor hosts. These are now discussed in more detail.

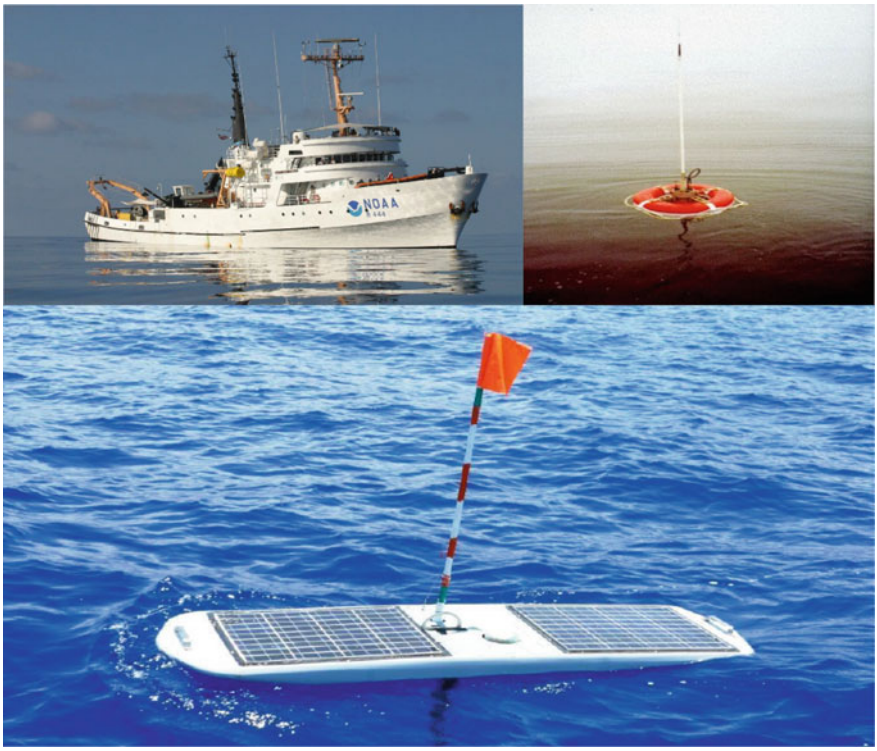

Fig. 5.2 Potential maritime hosts for infrasound sensing: ships (top left), ocean buoys (top right), and unmanned surfaces vehicles (bottom)

5.4.1 Ships

Of the possible maritime host platforms, ships have the highest mobility, allowing for relocation of the sensor to different areas of the ocean in the least amount of time. The sensor will be subject to heave, pitch, roll, ship vibration, and engine noise—all potential negative impacts on sensor performance. Onboard ships, there may be more options available to mitigate the effect of wind with ample deck space available, such as through intelligent sensor placement and the design of larger shrouds or distributed inlets such as can be obtained using long, perforated hoses. The practicality of using a set of ships to form an infrasound array is dubious because they must operate in close proximity, they are hugely expensive to operate, and will surely have higher priority tasking, making them unsuitable for affordable, persistent infrasound sensing missions. This leads us to consider unmanned host platforms, like ocean buoys and USVs.

5.4.2 Ocean Buoys

Normally, ocean buoys are moored to the ocean bottom and could potentially provide a persistent, autonomous, but nonmobile infrasound monitoring option. They would be subject to heave, pitch, and roll, and some lateral drift, constrained by the mooring's watch circle, but would likely experience less vibration and seismic interference than ships. Wind mitigation efforts may be more challenging due to the limited buoy real estate and the continuous exposure to the environment. Multiple moorings in the close proximity suitable for an infrasound array (hundreds of meters) may be prohibitive due to the risk of tangling and the array shape will dynamically change due to ocean current drift and winds. Normally, buoys will be subject to ocean surface waves and swell, resulting in sensor heave, pitch, and roll. A Spar buoy is a type of buoy with a tall, thin shape and which is very stable in the ocean, and much less sensitive to heave, pitch, and roll, creating a better potential platform for an infrasound sensor. A complication with any buoy is that deeper water greatly increases the difficulty of establishing and maintaining a buoy mooring, reducing the amount of available deployment area in the oceans. Drifting buoys, on the other hand, would be easier to deploy, but difficult to control location and to maintain the proximity needed for a multi-sensor array configuration.

5.4.3 Unmanned Surface Vehicles

Since around the early 1990s, there has been a large amount of development and innovation in the area of unmanned surface vehicles (Motwani 2012; Manley 2008). Development of USVs began with existing ships being outfitted with remote controls. Over time, smaller USVs have been developed, ranging from small ships to rigid-hulled inflatable boats (RHIBs) to platforms less than 10 feet long. The initial uses for USVs were military in nature, but now that the technology has matured, and smaller, cost-effective platforms can be secured, missions for civilian purposes, by industry and academia, are on the increase. The advantages of such systems are that the platforms can remain unmanned, are low cost (relative to manned ships), require no moorings, are mobile, and can perform various useful missions, including environmental surveys and remote sensing missions.

USV technology has moved from being remotely operated vehicles (ROV) to autonomous systems that perform tasking with a minimum of human interaction. Some USVs are now capable of harvesting wave, wind, and solar energy to provide their propulsion and power their systems and payloads. This is a significant development because it enables persistent operations without recovery, refueling, or maintenance. Such systems have the potential to operate in an unmanned state, conducting missions, for up to a year in duration. This emerging technology offers the opportunity to develop USV host platforms for infrasound sensing in the

maritime environment. Figure 5.3 shows example USV platforms which have been developed.

Table 5.1 compares ships, buoys, and USVs as potential maritime host platforms for the infrasound sensing application. Ship solutions are not deemed feasible for dedicated infrasound data collection because of the prohibitive expense and the improbability of being available during times of particular interest. Conventional

Fig. 5.3 Examples of Unmanned Surfaces Vehicles: DARPA's Sea Hunter, (top left), Ocean Aero's Submaran (top right, Copyright Ocean Aero Inc. Used with permission.), AutoNaut (bottom left, Copyright AutoNaut Ltd, with permission), ASV Global C-Enduro (bottom right, Copyright ASV Global, used with permission)

Table 5.1 Potential performance indicators for different maritime platforms

Parameter	Ships	Conventional buoys	Small USVs
Motion	Significant	Significant (unless Spar buoy)	Significant
Vibration problem	Significant	Minimal	Minimal
Wind problem	Low	High	High
Forming an array	Costly	Difficult	Possible
Platform autonomy	No	Yes	Yes
Platform mobility	High	None	Medium
Sensor survivability	High	Challenging	Challenging
Persistence	Low	High	Medium

ocean buoys are an option; they can be made persistent but it would be difficult to configure multiple buoys to form an array. Small USVs offer good persistence and the possibility of forming arrays due to control over their position. Ocean heave and wind noise will be challenging technical problems to solve for all three types of host platforms.

5.5 The Impact of Ocean Heave on Infrasound Data Collection in the Maritime Environment

Infrasound waves are longitudinal acoustic pressure waves. Infrasound pressure fluctuations for sources of interest are small compared to the ambient pressure. The ambient pressure at sea level is referred to as the atmospheric pressure (or hydrostatic pressure), which is due to the accumulated weight of the air in all of the atmospheric layers above; its nominal value is 101,325 Pa (or 1 atm). The received pressure wave signals for various infrasound sources range from about 5,000 to 1,000,000 times smaller than the ambient pressure. Ambient pressure decreases with altitude according to

$$P = P_0 \left(1 - \frac{Lh}{T_0}\right)^{\frac{gM}{RL}}, \tag{5.2}$$

where P_0 is sea level atmospheric pressure in Pa, h is the altitude in m, L is the temperature lapse rate for dry air in K/m, T_0 is sea level temperature in degrees Kelvin, g is gravitation acceleration in m/s^2, M is the mass of dry air in kg/mol, and R is the universal gas constant (8.31447 J/(mol K)) (Standard Atmosphere 1976).

Near sea level, where the infrasound sensor is to be located, changes in pressure due to slight changes in ocean heave can simply be approximated by the change in the force of gravity per area of air with given density as the volume of air above the sensor changes due to changing height, yielding

$$\Delta P = -\rho g \Delta h, \tag{5.3}$$

where ρ is the air density in kg/m^3. For a standard atmosphere (1 atm and 0 °C), $\rho = 1.2754$ kg/m^3, and

$$\frac{\Delta P}{\Delta h} \approx -12.5 \frac{\text{Pa}}{\text{m}} \tag{5.4}$$

That is, at sea level the pressure gradient with altitude is approximately −12.5 Pa/m. The implication is that an infrasound sensor, deployed in the maritime environment and moving vertically up and down (heaving) with ocean swell, will also be subject to pressure fluctuations due to changes in ambient atmospheric pressure. This heave-induced pressure change may be of significant strength given

typical sea surface swell of 1–2 m, with greater swells possible. It appears as an infrasound signal even though it is not, and it has the potential to obscure and interfere with the detection of actual infrasound signals-of-interest. If the heave-induced signal and the infrasound signal-of-interest occupy different and disjoint frequency bands, applying standard filtering methods will be successful in separating them. However, if the heave frequency spectrum and the infrasound signal spectrum overlap in frequency, then a more sophisticated heave compensation method must be applied, as described later. In addition, there is the possibility of additional pressure fluctuations due to non-propagating evanescent wave effects very near the ocean surface. However, the magnitude and impact of this potential effect for our sensor in the ocean environment require further study.

5.5.1 Sea Surface Characteristics

Tides produce cyclical changes in ocean water levels due to the gravitational forces of the moon and sun, the earth's rotation, and other factors. A common tidal effect is a semi-diurnal or diurnal period of fluctuation of several feet of water level, and it depends largely on geographic location and the moon's orbit. However, the frequency of a semi-diurnal tide is about once every 12 h, or 2.3e−5 Hz, which is well below the infrasound band propagation lower limit of around 0.003 Hz. Therefore, although an infrasound sensor exposed to tidal effects will experience ambient pressure fluctuations due to tidal heave; these can easily be ignored or filtered out since there are no infrasound signals-of-interest that low in frequency. Additionally, many infrasound sensors are AC-coupled to remove slowly varying pressure fluctuations below the infrasound measurement band.

Ocean surface roughness is driven by wind. When winds of certain speed and direction are sustained over enough time, the ocean surface becomes what is termed a "fully developed" sea. Wave size increases with increasing wind speed and increased the duration of the wind. The Beaufort scale (www.metoffice.gov.uk/corporate/library/catalogue.html; Petersen 1927) is an empirical table of sea conditions ("sea state") versus wind speed which is commonly used by seafarers. Beaufort numbers range from 0 (calm conditions) to 12 (hurricane conditions), increasing through breezes to strong wind to gales in between, with wave heights correspondingly increasing (over a range from 0 to 15 m). For the maritime infrasound application, it is important not only to understand the magnitude of ocean wave heave that the sensor will be subject to, but also the ocean wave frequencies (swell periods) associated with them.

The sea surface roughness can be characterized as a superposition of many waves with different periods (frequencies), heights, and directions. There may be more than a single source contributing to the generation of waves at any given location. Oceanographers typically use sea surface spectra to characterize the wave energy in the ocean as a function of frequency (and sometimes direction). The frequencies of the sea surface roughness (waves) are inversely related to the period

of the swell (i.e., $T_p = 1/f$). "Seas" often refer to localized, chaotic waves with many periods (broad frequency spectra), and can be distinguished from "swell", which is a well-behaved undulation (narrow spectral peak) that has propagated from longer distances. Oceanographic wave buoy instruments are commercially available which produce sea surface spectra by direct measurement of ocean heave (http://www.datawell.nl/Home.aspx; http://axystechnologies.com/). Predictions of sea surface spectra can be made using models, for assumed wind speeds. The Pierson–Moskowitz model is a simple, effective model which provides insight into the effects of sea surface roughness as a function of wind speed (Pierson and Moskowitz 1964), though more complicated models also exist (Hassellmann et al. 1980). Pierson–Moskowitz models a fully developed sea with a sea surface spectrum of the form:

$$S(\omega) = \frac{\alpha g^2}{\omega^5} e^{-\beta(\omega_0/\omega)^4}, \tag{5.5}$$

where α and β are dimensionless constants given by 7.79×10^{-3} and 0.74, respectively; g is gravitational acceleration. The reference frequency is given by $\omega_0 = g/U$, where U is the wind speed at a reference height of 19.5 m (often a reference of 10 m is also used).

Figure 5.4 shows examples of Pierson–Moskowitz spectra, which are observed to increase in peak energy level, become more peaked, and shift to lower frequencies at higher sustained wind speeds. Other useful parameters can be derived from the spectra, such as the predominant wave period (corresponding to the spectral peak) and the "significant wave height" (referred to as $H_{1/3}$ or H_s), which is the mean trough-to-crest wave height of the highest third of waves. This is a commonly used oceanographic parameter, which is consistent with what human observers estimate while at sea. Most wave heights will be less than $H_{1/3}$, but occasionally waves may be much higher. The mean wave height is approximately 0.7 times $H_{1/3}$ (Holthuijsen 2007). These parameters are shown in Fig. 5.5 for various wind speeds.

The ocean will cause the sensor to heave up and down by the magnitude of the wave heights and over a frequency band corresponding to the sea surface spectrum. Most sea surface spectra show that wave energy is contained within a frequency band of 0.03–0.3 Hz (which corresponds to wave periods of approximately 3–30 s). Networks of coastal and open-ocean oceanographic buoys provide web access to real time and historical data, including wind speed/direction, sea surface spectra, etc. (http://cdip.ucsd.edu/; http://www.ndbc.noaa.gov/); Fig. 5.6 shows various historical sea surface spectra, as measured from the Scripps Institute of Oceanography Coastal Data Information Program (CDIP) ocean buoy #067 (http://cdip.ucsd.edu/). Four different measurements are shown for different seasons, with different weather conditions. The 2013 spectra (blue and red) show low total energy and a broad spectrum of wave frequencies. The Jan 2014 spectrum shows a mix of two distinct swells. The April 2014 spectrum shows a single, very strong, long

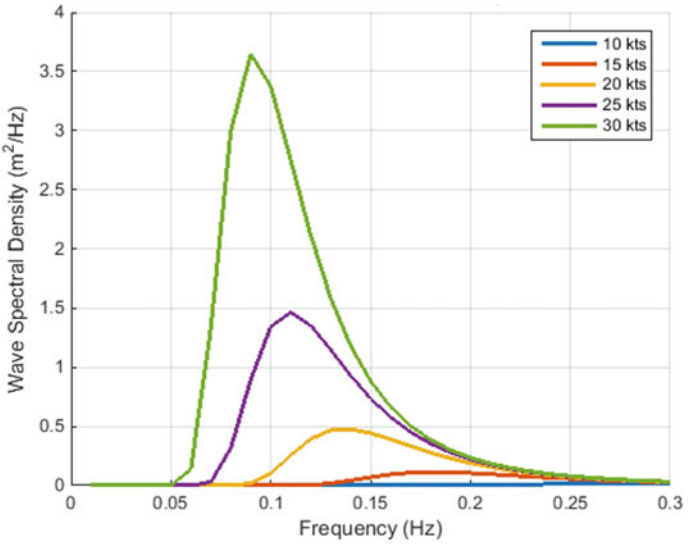

Fig. 5.4 Pierson–Moskowitz sea surface spectra for various wind speeds

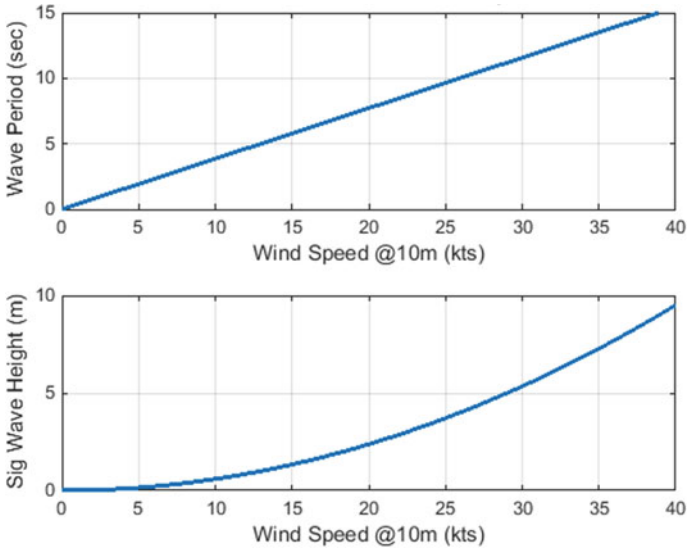

Fig. 5.5 Pierson–Moskowitz-predicted wave period and significant wave height as a function of wind speed

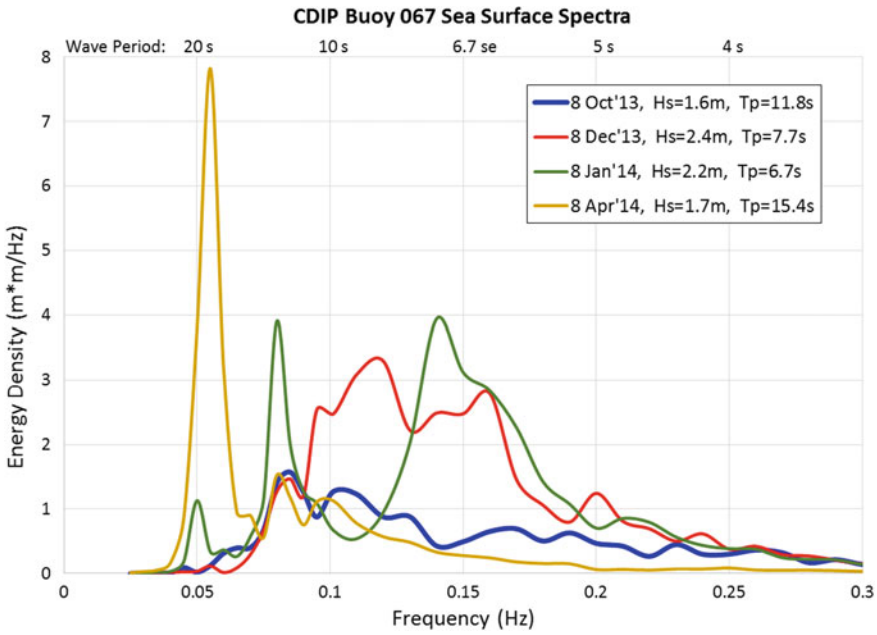

Fig. 5.6 CDIP Buoy 067 Sea Surface Spectra measurements

wave period swell. The significant wave height and wave period of the spectrum peak is also indicated.

As shown, both predictions and measurements indicate the ocean heave frequencies will be predominately within the 0.03–0.3 Hz frequency band. This wave energy band is directly within the infrasound band, and, therefore, the potential exists that ocean heave-induced pressure fluctuations sensed by a maritime infrasound sensor will interfere with the monitoring of infrasound signals-of-interest that are within this band, as depicted in Fig. 5.7. In fact, not surprisingly, the ocean heave frequency band overlaps with the microbarom band, as they are both driven by the same oceanographic effect. This also overlaps with the band used to monitor for nuclear explosions, potentially obscuring them from being detected. If the frequency content of the infrasound signal-of-interest and the sea surface spectrum band do not overlap in frequency, signal processing with conventional filtering techniques (low- or high-pass filtering) will adequately be able to separate the infrasound signals from the interfering heave-induced signals. However, if their spectra overlap, there will be interference unless the sensor heave is mitigated or compensated for in some manner.

This discussion is focused on the infrasound interference signal due to heave (N_{heave} in Eq. 5.1). As is clearly understood from the previous discussion, sea surface roughness is correlated to winds. Independent of heave interference, wind noise (N_{wind} in Eq. 5.1) will be another significant limiter to detection performance. However, the wind noise at the sensor location will be determined by the strength of

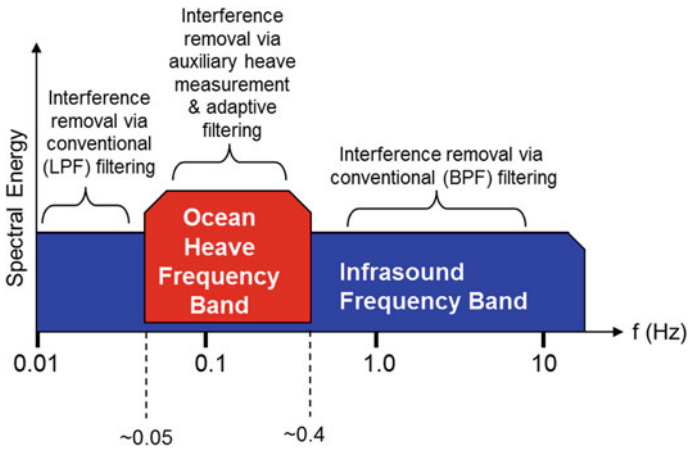

Fig. 5.7 Ocean heave contamination of the infrasound band

local winds, not necessarily the winds which produced the swell, which may have been generated by winds at great distances away. For example, the swell of April 2014 in Fig. 5.6 is a single, clean, long-period swell which was presumably generated far away and propagated a long distance to the sensor, where local winds may be calm. Also, there is a latency effect: swell is generated only after sustained winds exist for an adequate amount of time, and it dies away some time after the generating winds have died off. Thus, it is entirely possible for a sensor to experience large wave motion, yet not be overcome by wind noise.

5.5.2 *Ocean Heave Mitigation*

A proposed solution to the heave interference problem is to obtain an independent measurement of the infrasound sensor's heave as a reference signal to cancel the heave-induced pressure fluctuation from the infrasound sensor's signal. This is done by using a collocated inertial measurement unit (IMU), which tracks sensor motion, usually with 3-axis accelerometers and 3-axis gyros, and can independently compute accurate measurements of heave motion while being insensitive to other infrasound signals. This measurement should be highly correlated to the heave-induced interference pressure, and therefore can be used in an adaptive noise cancellation algorithm (Widrow and Stearns 1985); Fig. 5.8 shows a block diagram of such a process. The microbarometer senses the pressure signals originating from an infrasound signal-of-interest ($SL_{SOI} - TL$, in Eq. 5.1), if present, the infrasound background noise level ($(N_{wind} - PG_{wind} - F_{wind}) \oplus N_{other}$, in Eq. 5.1), and the interfering pressure fluctuations resulting from ocean heave (N_{heave}, in Eq. 5.1). A noisy estimate of the heave is obtained via the external IMU and serves as a

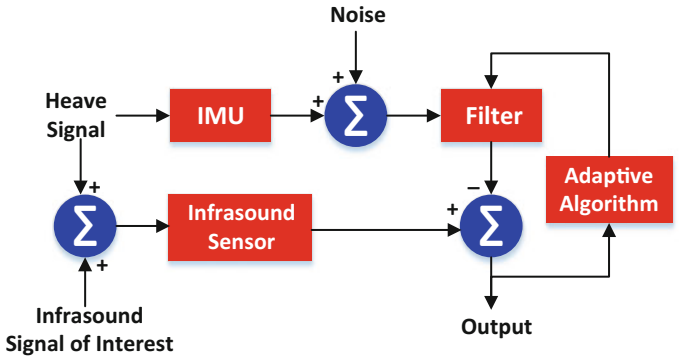

Fig. 5.8 Diagram of the interference cancellation filter algorithm

reference signal. The filter operates as a finite impulse response (FIR) filter with adjustable weights, and thus includes a tapped delay line of N samples (taps) of the IMU signal, which are each multiplied by an adjustable weighting coefficient. The sum of the weighted IMU samples is subtracted from the infrasound sensor sample to produce the system output. Successful subtraction, $N_{heave} - PG_{heave}$, depends on good correlation between the reference and heave pressure signals. The output is also supplied as an error signal to an adaptive algorithm through a feedback loop, which adjusts the weights of the adaptive filter to minimize the error for the next iteration of the filter's operation. There are a number of adaptive algorithms that can be used, including least mean squares (LMS) and recursive least squares (RLS) as two of the simplest and most common (Widrow and Stearns 1985). Proper tuning of the algorithm parameters is required to obtain optimal performance for a specific signal characterization. As the filter adapts using this feedback loop, it drives the output to be as small as possible, which corresponds to maximum removal of the correlated heave signal and the output more closely representing just the infrasound SOI ($SL_{SOI} - TL$) and/or the natural infrasonic background and wind noise ($([N_{wind} - PG_{wind} - F_{wind}) \oplus N_{other}]$, in Eq. 5.1).

5.6 Infrasound Data Collection and Heave Cancellation from Ship-Hosted Infrasound Sensor

Initial testing of the heave compensation method was performed with data collected during February, 2016, off the coast of Southern California, during an at-sea experiment. A Hyperion Inc. IFS-5000 microbarometer (com/wp-content/uploads/2013) originally developed by the National Center for Physical Acoustics (NCPA) was fielded onboard the R.V. Acoustic Explorer (AX) research vessel, shown in Figs. 5.9 and 5.10. The microbarometer was installed on the upper afterdeck of the AX, nearly above the ship's center of rotation (COR) to reduce any negative effects

Fig. 5.9 Acoustic Explorer research vessel

Fig. 5.10 The Hyperion IFS-5000 microbarometer sensor (left) and the SBG inertial measurement unit (right)

of pitch and roll. In addition, an SBG Ekinox-A AHRS (attitude, heading, reference system) IMU (https://www.sbg-systems.com/products/ekinox-high-performance-mems-ahrs), shown in Fig. 5.10, was installed in close proximity to the microbarometer, within about 1–2 feet. Any residual distance offset between the IMU and COR was measured and programmed into the IMU firmware to be accounted for in its heave calculation algorithm. The ship deployed and these sensors recorded for about a 1 week period. Sea conditions during the period were low, with swell causing heave fluctuations of usually less than 0.5 m.

A representative 5-min segment of microbarometer pressure and IMU heave data was selected for a heave cancellation analysis. The raw microbarometer pressure and IMU heave timeseries data were low-pass filtered below 0.5 Hz in order to isolate the effect of heave from other higher frequency acoustic energy which may have been present in the data (and which can be recovered via normal band pass filter methods because they are out of the heave band). The pressure and heave (IMU) time series were resampled to have a common sample rate of 25 Hz, which is oversampled by a factor of about 10. The heave data were converted from distance units (meters) to pressure units (Pa) using the relationship in Eq. 5.4. Figure 5.11 shows a comparison between a 120-s segment of the pressure and heave signal time series. The performance of the adaptive cancellation filter is dependent upon the degree to which the two signals are correlated (Grimmett and Zabal 1993). The normalized correlation function was computed between these signals and the peak correlation coefficient was found to be 0.97; this high degree of correlation is also visually evident in the time series. There is a small difference in amplitude due to the fact that the conversion of the IMU heave from meters to pressure is based on an average approximation (Eq. (5.4)), not a location/time-specific value, in addition to measurement inaccuracies of both the microbarometer and IMU, the latter of which has a maximum accuracy of 2.5 cm of heave. However, this is easily compensated for by the filter taps of the adaptive filter. Their spectra, computed over the entire 300-s time window, are shown overlaid in Fig. 5.12, and are also seen to be very similar within the ocean heave band. It is clear for this data segment that the heave is sufficiently strong to be a dominant effect, potentially obscuring other quieter infrasound signals that may be present.

In order to assess and quantify the performance of the algorithm, we choose to inject an artificial signal to represent our infrasound signal-of-interest (SOI). Doing this also facilitates being able to quantitatively assess the algorithm's performance under different SOI sound pressure levels. For the artificial signal, we chose one that occupies a similar frequency band as the actual heave which was present during the experiment. Although, in general, the SOI would be generated from an event other than ocean heave, for this analysis we have obtained a separate, uncorrelated ocean heave measurement obtained from an ocean monitoring buoy which is a part of the CDIP network (http://cdip.ucsd.edu/) to use as our SOI due to ease of availability and guarantee of the desired frequency content within the heave band. Figure 5.13 shows a portion of the artificial SOI compared to the microbarometer-received signal. Note that we choose to inject the signal only after 60 s, with no signal injected during the first minute of the data used in this analysis. This will enable us to understand the performance of the algorithm when there is no SOI present. In this figure, the SOI has been amplitude scaled so that it has equivalent power as the heave-dominated microbarometer pressure signal, i.e., a SOI-to-Heave ratio (SHR) of 0 dB. The normalized correlation coefficient between the nonzero portion of the injected SOI and the sensor pressure signal was 0.27, and is clearly observed to be uncorrelated. Figure 5.14 shows a comparison of the two signals' spectra, which shows that although they occupy the same frequency band,

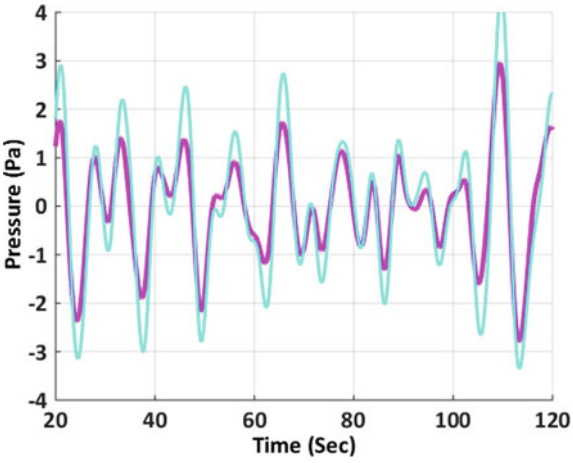

Fig. 5.11 Microbarometer pressure signal time series (magenta) and IMU heave signal time series (cyan) selected for analysis

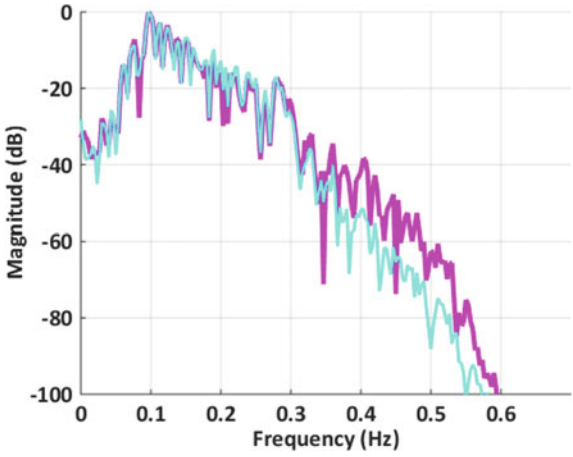

Fig. 5.12 Microbarometer pressure signal spectra (magenta) and IMU heave signal spectra (cyan) corresponding to the signals in Fig. 5.11

they do not share a similar, detailed spectral structure, even within the ocean heave band.

The artificial SOI is injected into the data set by summing with the received microbarometer pressure signal, as shown in Fig. 5.15 (green curve). This composite signal is composed of: the as-yet unobservable infrasound background noise, the heave-induced pressure signal, and the injected artificial SOI with a signal-to-heave ratio of 0 dB (shown over the interval from 60 to 120 s). Before 60 s we see that the composite is just the microbarometer signal, which is dominated by the heave effect. This composite signal serves as the input to the adaptive noise cancellation system. The IMU heave measurement is fed to the system as the reference signal (the cyan curve from Fig. 5.11). The RLS algorithm was used to update an adaptive filter with a length of 11 taps. The RLS algorithm has an exponential weighting, or forgetting factor, $0 < \lambda < 1$, which defines how much to

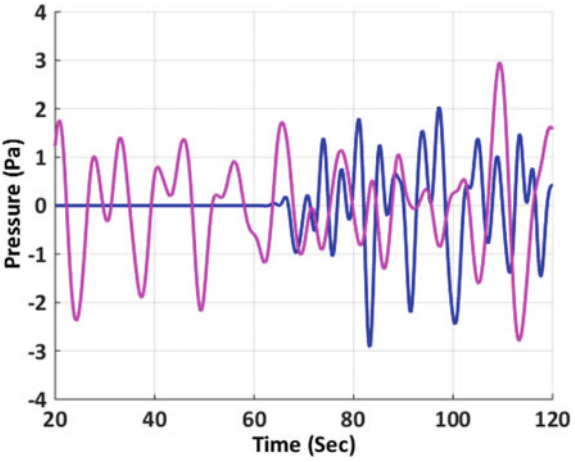

Fig. 5.13 Time series of the artificial infrasound signal-of-interest (SOI) (blue), SHR = 0 dB, injected after 60 s, compared to the microbarometer pressure signal time series (magenta)

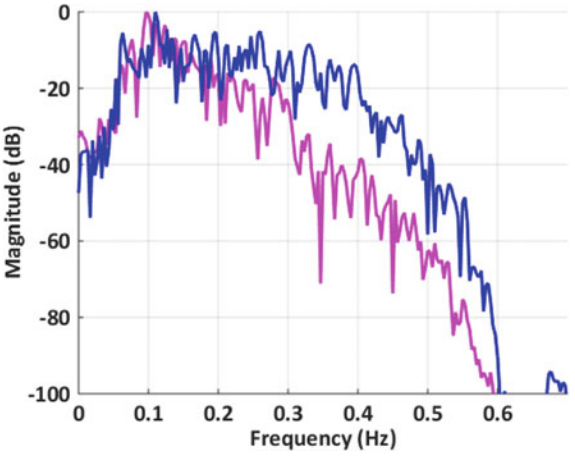

Fig. 5.14 A comparison of the spectra of the artificial infrasound SOI (blue) and the microbarometer pressure signal (magenta), corresponding to the time series signals in Fig. 5.13

weight past samples versus the current sample. It is approximately equivalent to a sliding window of length $\frac{\lambda}{1-\lambda}$ samples. In this case, a value of 0.9999 has been used, corresponding to approximately 10,000 samples, or 400 s at the 25 Hz sample rate.

The output of the adaptive filter is compared with the input signal in Fig. 5.16. The result shows effective cancellation of the heave-induced pressure component, while the injected SOI has been recovered. The residual output signal seen before 60 s is likely the actual infrasound noise background without the interference of ocean heave. Figure 5.16 compares the injected SOI and the adaptive filter's output. In this example, the cancellation algorithm has effectively recovered the SOI (shown over the interval from 60 to 120 s) and revealed its estimate of the true (heave less) infrasonic natural and wind noise background (before 60 s).

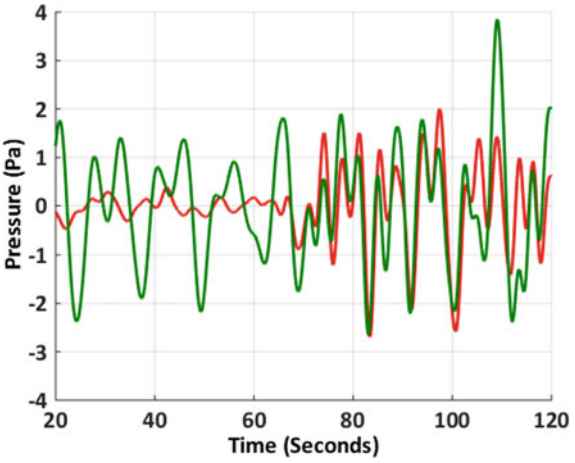

Fig. 5.15 Comparison of the composite signal (with injected artificial infrasound SOI of equal power to heave, SHR = 0 dB) input to the adaptive cancellation filter (green) and the filter's output (red)

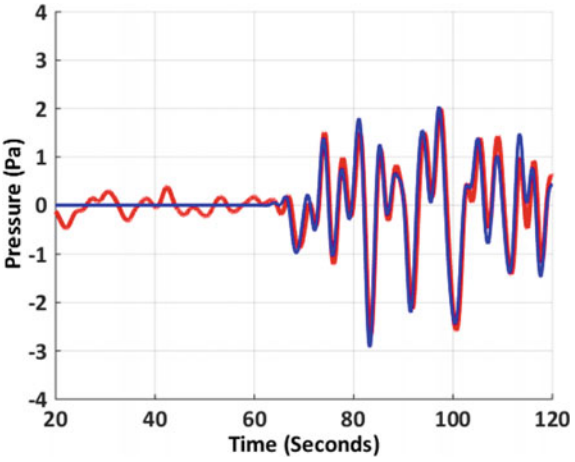

Fig. 5.16 A comparison of the injected infrasound SOI, SHR = 0 dB (blue) and the adaptive cancellation filter's output (red)

Figure 5.17 shows the filter input and output when the SOI has been reduced in power by 9 dB relative to the previous example. Here the filter's input looks very nearly identical to the heave-dominated sensor pressure signal, since the SOI is small. The output shows that the SOI has been recovered and that it is still detectable above the infrasound noise floor. Figure 5.18 shows the similarity of the injected SOI and the recovered SOI. Finally, we run the adaptive cancellation filter without injecting any SOI; Fig. 5.19 shows the heave-dominated pressure signal input and the estimated, heave-less infrasound noise background. The algorithm's heave power reduction is found to be about 14 dB, for the conditions of this experiment, with the given infrasound noise floor level, and the heave fluctuations that were limited to less than 0.5 m.

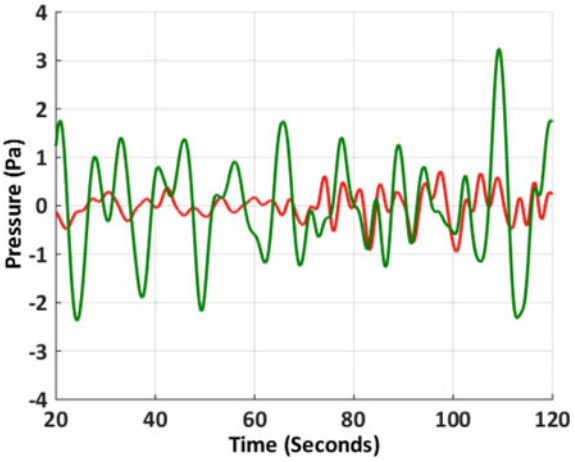

Fig. 5.17 Comparison of the composite signal (with injected artificial infrasound SOI of 1/8 the power of the heave, SHR = −9 dB) input to the adaptive cancellation filter (green) and the filter's output (red)

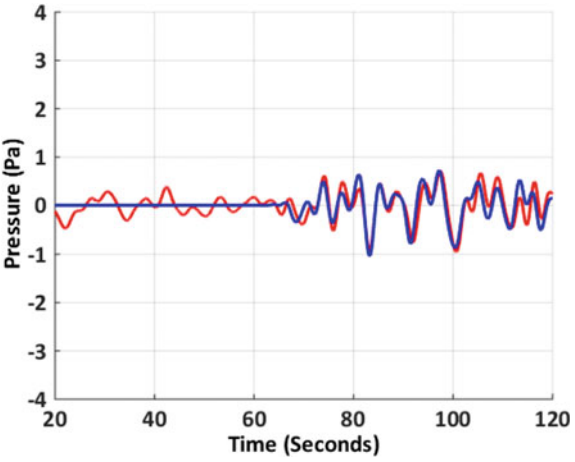

Fig. 5.18 A comparison of the injected infrasound SOI (blue) and the adaptive cancellation filter's output (red), for the data in Fig. 5.17

In order to fully characterize the performance of the heave cancellation algorithm, we now scale the injected SOI over a range of SOI-to-Heave ratios to characterize the effectiveness of SOI recovery and heave cancellation. The input signal SHR is varied by doubling the SOI mean power (via 3 dB steps) from −24 dB to +12 dB relative to the heave-dominated pressure signal (SHR = 0 dB implies the equal power case presented in Figs. 5.8, 5.9, 5.10 and 5.11). For each of these cases, we evaluate the cancellation performance.

Figure 5.20 shows the acoustic power levels of the various signals in the processing, in dB relative to the power of the heave. Three regimes are indicated: power of the SOI less than the power of the noise background ($P_N > P_{SOI}$), power of the SOI greater than the power of the heave interference ($P_{SOI} > P_H$), and power of the SOI greater than noise power but less than the heave interference ($P_N <$

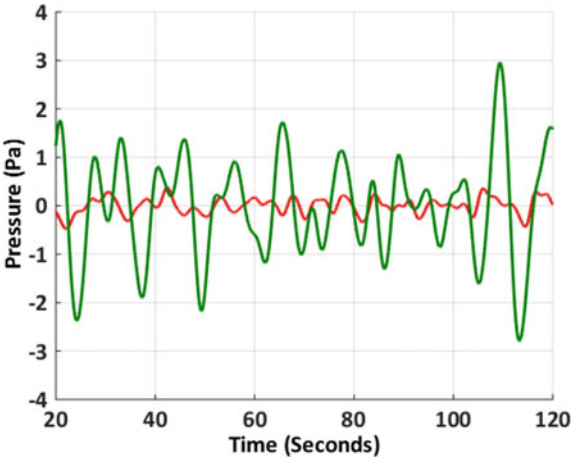

Fig. 5.19 Comparison of the composite signal (without any injected artificial infrasound SOI, SHR = −Inf dB) input to the adaptive cancellation filter (green) and the filter's output (red)

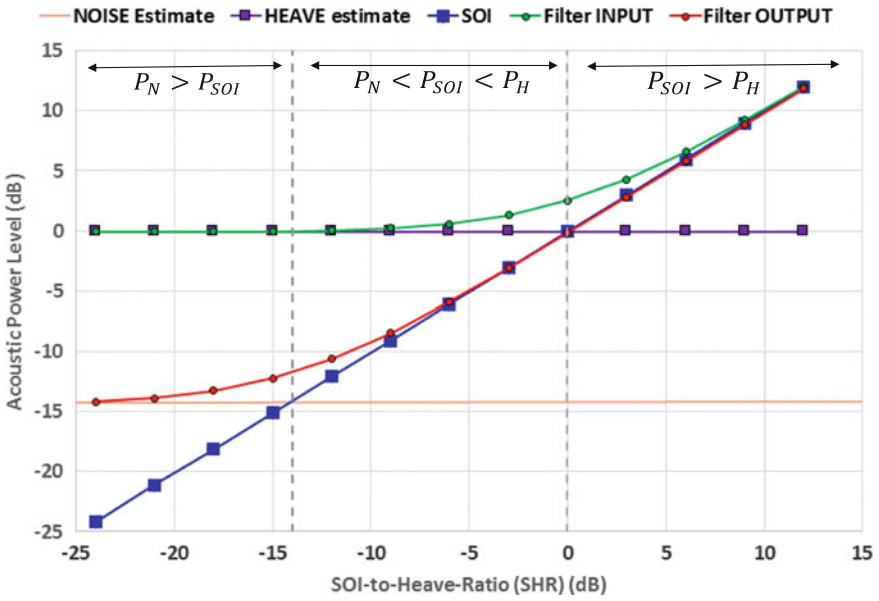

Fig. 5.20 Mean acoustic power levels as a function of the SHR. The filter input (green) is the composite (power sum) of the noise floor (orange), the heave (purple), and the SOI (blue). The output (red) is shown for three regimes: SOI power below the noise, SOI power above the heave, and SOI between the noise and the heave

$P_{SOI} < P_H$). The heave interference power is shown to be constant at 0 dB and the filter output noise background was determined to be −14 dB. This was estimated by measuring the amount of suppression achieved by the filter when no SOI was injected.

The filter input signal is the composite (power sum) of the acoustic noise background, the heave-induced interference, and the SOI. We see that the filter input power is dominated by the heave, until the SOI power becomes equal to the heave. As the SOI power increases further in the regime $P_{SOI} > P_H$, the filter input signal becomes dominated by the SOI. Here, the SOI may already be strong enough to be detectable above the heave interference, however, the heave reduction algorithm will further increase its detectability. When dominated by the SOI, the filter's output signal has the heave removed while retaining the SOI, so its power is close to the power of the SOI. As the input SOI power drops in the regime $P_N < P_{SOI} < P_H$, we see that the filter is able to reduce the output power to the point that the SOI becomes dominant. In this regime, the SOI is not detectable at the input, but after applying the algorithm, it becomes detectable. When the input SOI power drops below the infrasound noise floor ($P_N > P_{SOI}$), the SOI is obscured by the infrasound noise floor and therefore will not be recoverable using this method, even when the heave has been reduced by its maximum amount. Other noise cancellation processes (e.g., beam forming, etc.) could be considered to improve detectability in this case, if multiple, appropriately spaced sensors are available.

The estimated noise level in Fig. 5.20 is actually a combination of three residual signals: unsuppressed heave, heave measurement noise, and infrasound background. The first consists of any remaining pressure fluctuations due to heave that were not removed by the adaptive filter. This is presumed to be small due to the lack of correlation between the input and output signals. The heave measurement noise is an artifact due to inaccuracies in both the microbarometer and IMU in capturing the vertical displacement of the platform. The infrasound background consists of actual sources of low-frequency pressure waves that exist in the environment. Because these are unknown, it is impossible for us to identify how much of the output signal power is due to each of these three components. Thus, it is important to understand that the 14 dB reduction in output power shown here is only a lower bound on the amount of heave suppression that has been achieved; the actual heave remaining in the output signal may, in fact, be much lower than, and dominated by, the measurement noise and/or the natural infrasound background. The SOI detectability (the difference between SOI and combined obscuring signals) is always improved by the same amount (14 dB in our case) regardless of injected SOI level, despite the fact that the output power is affected less and less as SOI level increases due to its detectability being higher to begin with. The amount of detectability improvement possible with this algorithm will depend on the difference between the power levels of the data's heave interference (due to ocean swell) and the infrasound noise background, as well as how correlated the filter reference signal is with the heave content in the data and how well the algorithm is tuned. The detectability improvement observed will depend on the SOI level with respect to the amount of combined background noise of the three aforementioned sources.

5.7 Infrasound Data Collection and Heave Cancellation from USV-Hosted Infrasound Sensor

Another experiment was conducted to collect infrasound data from a USV platform, rather than from a ship. The Hyperion microbarometer and SBG IMU (described previously) were installed on a Liquid Robotics Wave Glider SV-2 USV (http://liquidr.com/). The Wave Glider is composed of a surfboard-sized surface float and a subsurface glider unit, as shown in Fig. 5.21. The surface float provides GPS and navigation, communications gear, space for payload electronics, and solar panels for electrical power. The unit harvests wave energy for propulsion; as the ocean heave draws the float up and down, the tension with the glider unit provides forward propulsion. The unit can be navigated remotely through a server connected to the internet. It is persistent and can remain on a mission for up to one year, traveling at speeds of 0–1.5 knots.

Figure 5.22 shows the Wave Glider with the microbarometer installed on a slightly raised platform. A colander is put over the top of the Wave Glider to act as a shroud and provide some wind noise reduction for the sensor. The sensor was also

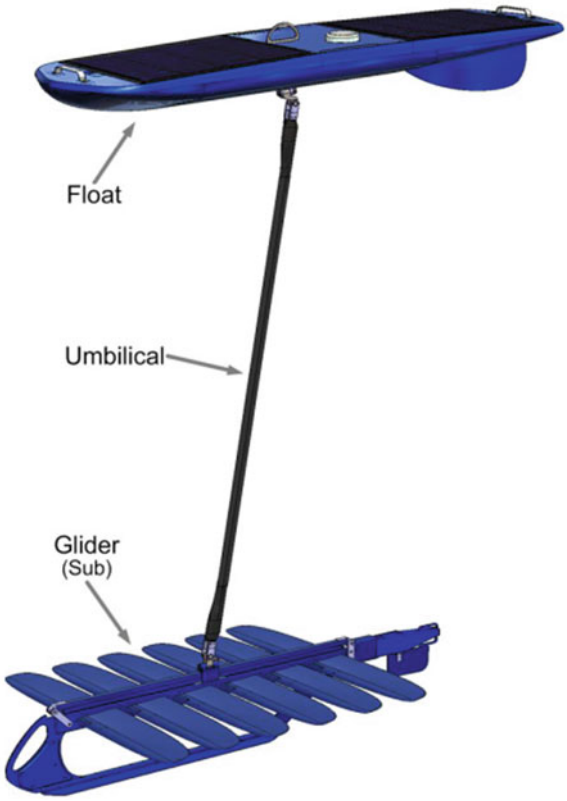

Fig. 5.21 The Wave Glider® SV2—designed and manufactured by Liquid Robotics, Inc. Image used with permission

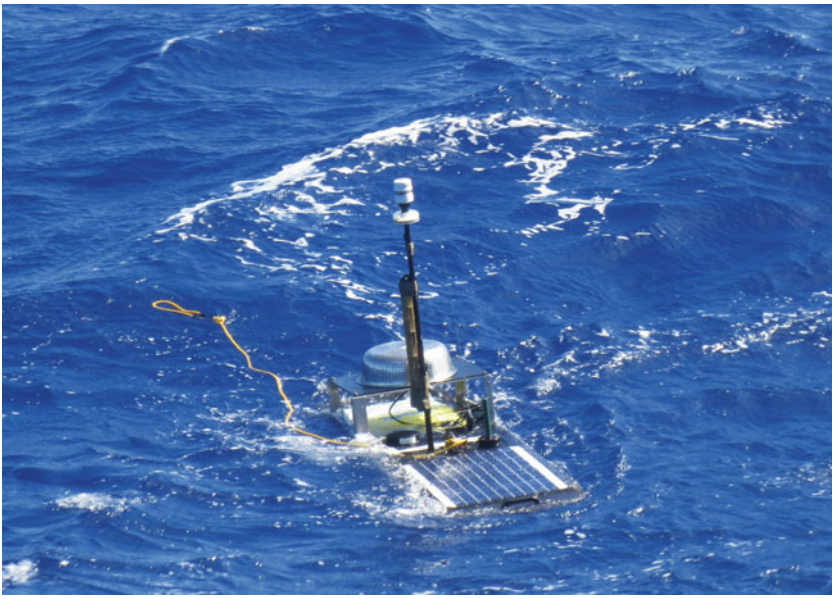

Fig. 5.22 The USV-hosted infrasound sensor configuration

wrapped in open cell, nearly acoustically transparent foam to further reduce wind noise and to provide some resistance to water penetration. The IMU and data collection electronics were housed inside the float in a payload bay. The mast hosts GPS and Iridium satellite communications antennas. The system was deployed for operations for 1 day in the Pacific Ocean off the coast of Hawaii and was piloted remotely. Data was collected and the instrument performance was evaluated. The sea conditions produced swell of about 0.5–1.5 m over the data collection period.

An analysis similar to that done with the ship-hosted experiment was performed to demonstrate the heave cancellation. Here the injected SOI was chosen to be an infrasound detection of the Chelyabinsk meteor event, which occurred in February 2013. This event was detected by many infrasound stations around the world. Time series data of this event, detected by a single microbarometer in the USArray TA (Station G42A, LDF channel located in Wisconsin, U.S.A.), was obtained from the Incorporated Research Institutions for Seismology (IRIS) (http://www.iris.edu/hq/). Figure 5.23 shows a spectrogram of the Chelyabinsk infrasound event, from which a SOI was extracted, amplitude-scaled, and injected into the Wave Glider-hosted microbarometer data.

Figure 5.24 shows the microbarometer data (magenta) before SOI injection compared to the IMU signal (cyan) for a 200-s data segment. The extracted Chelyabinsk meteor signal was scaled into Pascals (from A/D counts, because sensor calibration information was not available) such that it would have equal power as the received microbarometer data, which are both shown overlaid in Fig. 5.25. These were then summed and the composite signal (SOI, heave, and infrasound

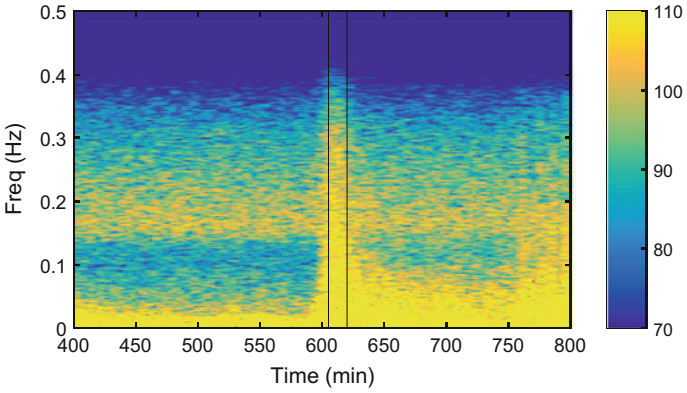

Fig. 5.23 Spectrogram of the Chelyabinsk meteor detection data (in dB), with a highlighted section from which a signal-of-interest was extracted, scaled, and used for algorithm demonstration

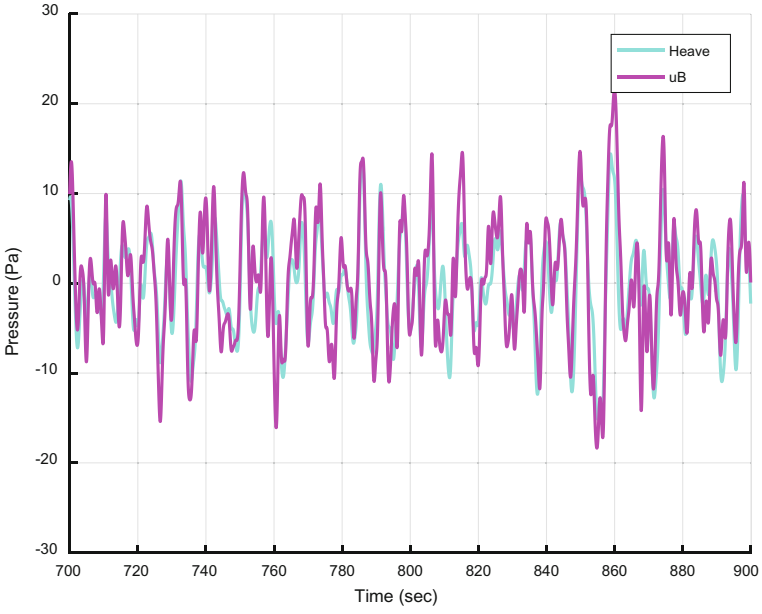

Fig. 5.24 The Wave Glider-hosted microbarometer data (magenta) compared to the heave signal (cyan)

background) was input to the adaptive heave cancellation filter. The results are shown in Fig. 5.26, where reductions in the heave are evident. Figure 5.27 compares the injected SOI with its recovered version after adaptive filtering and reasonable results are obtained.

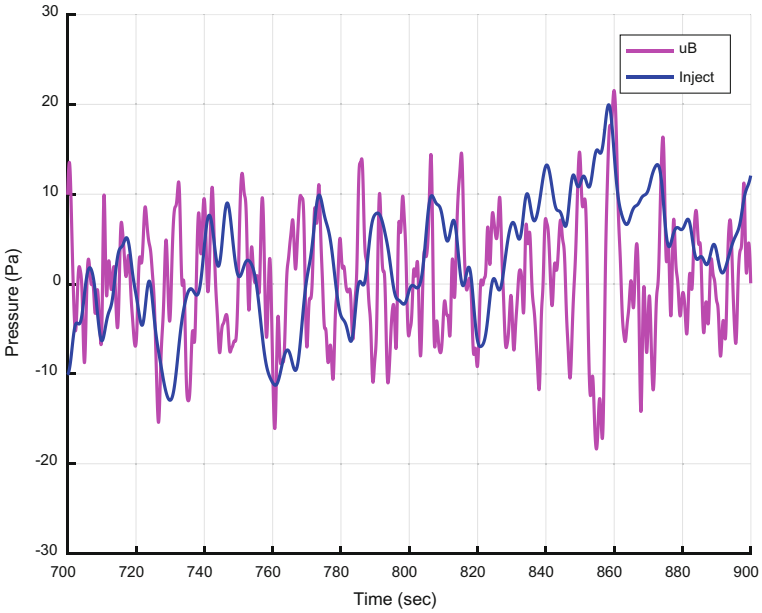

Fig. 5.25 The microbarometer data (magenta) and the injected, scaled Chelyabinsk signal (blue)

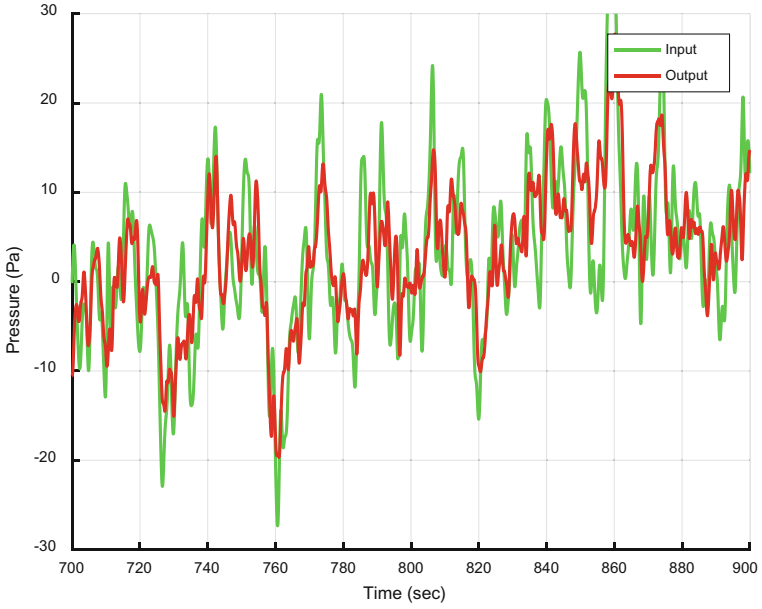

Fig. 5.26 The adaptive heave cancellation input (sum of scaled Chelyabinsk signal and microbarometer signal, in green), and algorithm output (red)

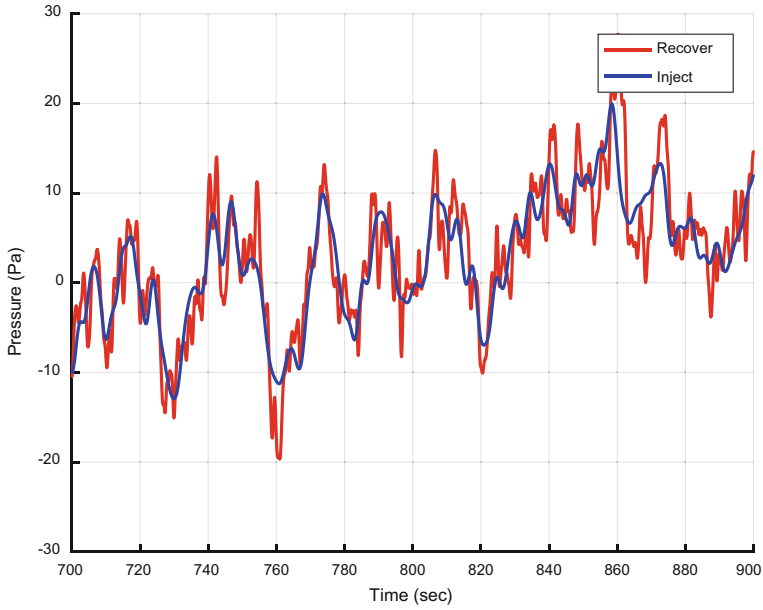

Fig. 5.27 The injected, scaled Chelyabinsk signal (blue) and algorithm output signal (red) showing the good recovery of the Chelyabinsk signal

5.8 Summary

Infrasound monitoring stations are normally land-based systems. The successful development of infrasound data measurement systems fielded in the maritime environment offers the potential to collect valuable infrasound data over the expansive oceanic areas of the globe. This can potentially augment land-based stations by providing improvements in detection and infrasound event coverage. In addition, it offers improvement in infrasound event localization, tracking, and classification/verification. The oceans offer the possibility of a denser worldwide network of infrasound sensing that would provide an increased understanding of the atmospheric effects and impacts on infrasound propagation.

To make maritime infrasound stations viable, various challenges must be overcome. The main foreseen challenges are: protecting and making the sensor survivable in the maritime environment, overcoming the negative effects of sensor motion due to ocean heave, ocean wind noise mitigation, and forming multi-element arrays of sensor while in the maritime. Work so far has focused on sensor survivability and sensor motion mitigation.

Actual deployments on the ocean have been accomplished onboard ship and USV host platforms. The USV deployments have been made over only short durations and in a limited set of ocean/environmental conditions. Better protection of the sensor will be required, such that it is open to the atmosphere but closed to

water. Improvements are being developed to provide a more robust weatherproofing to the system. While the sensors deployed on a ship were better protected from water and wind, they did suffer from significant ship noise and vibration. The USV implementation showed promise by providing a lower background noise floor than the ship. The heave interference signal has been prominent in data sets from both ship and USV, even though the ocean swell they were subject to was small. A potential solution to the ocean heave problem has been demonstrated on these data with an adaptive noise cancellation algorithm and the use of an external heave reference signal obtained from an IMU.

Further efforts are needed to validate this preliminary work undertaken so far, and to investigate solutions to remaining problems and answers to open questions. First, a characterization of the wind noise levels in the ocean environment is needed. Mitigation methods, including windscreens or multi-sensor cancellation methods are to be explored. Also, once performance on a single sensing node is determined to be adequate, we aim to demonstrate the capability of forming arrays of sensors in the ocean environment by configuring and sailing a small group of USVs.

Deployments over longer durations and in different ocean conditions are needed to assess reliability. Such a long-term deployment will provide opportunities for a demonstration of actual, attributable infrasound signal to be detected. Such efforts will continue to explore the feasibility and potential that a maritime infrasound sensing technology may offer.

Acknowledgements We acknowledge the SPAWAR Systems Center Pacific NISE program, which provided the required funding to perform this work. We acknowledge the managers, captain, and crew of the R.V. Acoustic Explorer ship for their experimental support in collecting the infrasound measurements used herein. We acknowledge Talmadge Carrick (National Center for Physical Acoustics) and Chad Williams (Hyperion Technology Group) for useful discussions and advice on sensor configurations during experimentation.

References

Assink J, Smets P, Marcillo O, Weemstra C, Lalande J-M, Waxler R, Evers L (2019) Advances in infrasonic remote sensing methods. In: Le Pichon A, Blanc E, Hauchecorne A (eds) Infrasound monitoring for atmospheric studies, 2nd edn. Springer, Dordrecht, pp 605–632

Axys Technologies. http://axystechnologies.com/

Bowman C, Lees J, Cutts J, Komjathy A, Young E, Seiffert K, Boslough M, Arrowsmith S (2019) Geoacoustic observations on drifting balloon-borne sensors. In: Le Pichon A, Blanc E, Hauchecorne A (eds) Infrasound monitoring for atmospheric studies, 2nd edn. Springer, Dordrecht, pp 125–171

Bratt SR, Bache TC (1988) Locating events with a sparse network of regional arrays. Bull Seismol Soc Am 78:780–798

Cansi Y (1995) An automatic seismic event processing for detection and location: the P.M.C.C. method. Geophys Res Lett 22(9):1021–1024

Ceranna L, Matoza R, Hupe P, Le Pichon A, Landès M (2019) Systematic array processing of a decade of global IMS infrasound data. In: Le Pichon A, Blanc E, Hauchecorne A (eds) Infrasound monitoring for atmospheric studies, 2nd edn. Springer, Dordrecht, pp 471–482

Christie DR, Campus P (2010) The IMS infrasound network: design and establishment of infrasound stations. In: Le Pichon A, Blanc E, Hauchercorne A (eds) Infrasound monitoring for atmospheric studies. Springer

Chunchuzov I, Kulichkov S (2019) Internal gravity wave perturbations and their impacts on infrasound propagation in the atmosphere. In: Le Pichon A, Blanc E, Hauchecorne A (eds) Infrasound monitoring for atmospheric studies, 2nd edn. Springer, Dordrecht, pp 551–590

Datawell BV. http://www.datawell.nl/Home.aspx

De Groot-Hedlin CD, Hedlin M (2015) A method for detecting and locating geophysical events using groups of arrays. Geophys J Int 203:960–971

de Groot-Hedlin C, Hedlin M, Drob D (2010) Atmospheric variability and infrasound monitoring. In: Le Pichon A, Blanc E, Hauchercorne A (eds) Infrasound monitoring for atmospheric studies. Springer

de Groot-Hedlin C, Hedlin M (2019) Detection of infrasound signals and sources using a dense seismic network. In: Le Pichon A, Blanc E, Hauchecorne A (eds) Infrasound monitoring for atmospheric studies, 2nd edn. Springer, Dordrecht, pp 669–699

Drob D (2019) Meteorology, climatology, and upper atmospheric composition for infrasound propagation modeling. In: Le Pichon A, Blanc E, Hauchecorne A (eds) Infrasound monitoring for atmospheric studies, 2nd edn. Springer, Dordrecht, pp 485–508

Drob DP, Meier RR, Picone JM, Garces MM (2010) The IMS infrasound network: design and establishment of infrasound stations. In: Le Pichon A, Blanc E, Hauchercorne A (eds) Infrasound monitoring for atmospheric studies. Springer

Frazier G (2014) Application of parametric empirical Bayes estimation to enhance detection of infrasound transients. Presentation of infrasound technology workshop 2014, comprehensive test ban treaty organization, Oct 2014

Green DN, Bowers D (2010) Estimating the detection capability of the International Monitoring System infrasound network. J Geophys Res 115:D18116. https://doi.org/10.1029/2010JD014017

Grimmett D, Zabal X (1993) Performance criteria for coherent interping reverberation suppression, Naval Command Control and Ocean Surveillance Center, RDT&E Division (NRAD), TD 2591, Dec 1993

Grimmett D, Plate R, Goad J (2016) Ocean Heave cancellation for a maritime infrasound sensor. In: Proceedings of the MTS/IEEE oceans'16 conference, Sept 2016, Monterey, California

Hassellmann DE, Dunckel M, Ewing JA (1980) Directional wave spectra observed during JONSWAP 1973. J Phys Oceanogr 10:1264

Holthuijsen LH (2007) Waves in oceanic and coastal waters. Cambridge University Press, p 70

Hyperion Technology Group. http://hyperiontg.com/wp-content/uploads/2013/08/IFS5000SpecSheet.pdf

Incorporated Research Institutions for Seismology. http://www.iris.edu/hq/

Le Pichon A, Ceranna L, Vergoz J (2012) Incorporating numerical modeling into estimates of the detection capability of the IMS infrasound network. J Geophys Res 117:D05121. https://doi.org/10.1029/2011JD016670

Le Pichon A, Ceranna L, Vergoz J, Tailpied D (2019) Modeling the detection capability of the global IMS infrasound network. In: Le Pichon A, Blanc E, Hauchecorne A (eds) Infrasound monitoring for atmospheric studies, 2nd edn. Springer, Dordrecht, pp 593–604

Liquid Robotics. http://liquidr.com/

Manley JE (2008) Unmanned surface vehicles, 15 years of development. In: Proceedings of the MTS/IEEE oceans 2008 conference, Sept 2008, Quebec City, Canada

Marty J (2019) The IMS infrasound network: current status and technological developments. In: Le Pichon A, Blanc E, Hauchecorne A (eds) Infrasound monitoring for atmospheric studies, 2nd edn. Springer, Dordrecht, pp 3–62

Meltzer A (1999) The USArray initiative. Geol Soc Am Today 9:8–10

Met Office, The Beaufort Scale, Fact sheet 6 (version 01), National Meteorological Library and Archive, Devon, United Kingdom. www.metoffice.gov.uk/corporate/library/catalogue.html
Mialle P, Brown D, Arora N, colleagues from IDC (2019) Advances in operational processing at the international data centre. In: Le Pichon A, Blanc E, Hauchecorne A (eds) Infrasound monitoring for atmospheric studies, 2nd edn. Springer, Dordrecht, pp 209–248
Motwani A (2012) A survey of uninhabited surface vehicles, Technical Report MIDAS. SMSE.2012.TR.001, Marine and Industrial Dynamic Analysis, School of Marine Science and Engineering, Plymouth University, PL4 8AA, United Kingdom
National Oceanic and Atmospheric Administration (NOAA), National Data Buoy Center. http://www.ndbc.noaa.gov/
Nief G, Talmadge C, Rothman J, Gabrielson T (2019) New generations of infrasound sensors: technological developments and calibration. In: Le Pichon A, Blanc E, Hauchecorne A (eds) Infrasound monitoring for atmospheric studies, 2nd edn. Springer, Dordrecht, pp 63–89
Petersen P (1927) Zur Bestimmung der Windstärke auf See. Annalen der Hydrographie und Maritimen Meteorologie 55:69–72
Pierson WJ, Moskowitz L (1964) A proposed spectral form for fully developed wind seas based on the similarity theory of A. A. Kitaigorodskii. J Geophys Res 69:5181–5190
Pilger C, Ceranna L, Ross JO, Le Pichon A, Mialle P, Garces MA (2015) CTBT infrasound network performance to detect the 2013 Russian fireball event. Geophys Res Lett 42:2523–2531. https://doi.org/10.1002/201sgl063482
SBG systems. https://www.sbg-systems.com/products/ekinox-high-performance-mems-ahrs
Scripps Institution of Oceanography, Coastal Data Information Program (CDIP). http://cdip.ucsd.edu/
U.S. Standard Atmosphere (1976) National Oceanic and Atmospheric Administration, National Aeronautics and Space Administration, United States Air Force, NOAA-S/T 76-1562, Oct 1976
Vergoz J, Le Pichon A, Millet C (2019) The antares explosion observed by the USArray: an unprecedented collection of infrasound phases recorded from the same event. In: Le Pichon A, Blanc E, Hauchecorne A (eds) Infrasound monitoring for atmospheric studies, 2nd edn. Springer, Dordrecht, pp 349–386
Waxler R, Assink J (2019) Propagation modeling through realistic atmosphere and benchmarking. In: Le Pichon A, Blanc E, Hauchecorne A (eds) Infrasound monitoring for atmospheric studies, 2nd edn. Springer, Dordrecht, pp 509–549
Widrow B, Stearns SD (1985) Adaptive signal processing. Prentice-Hall, Englewood Cliffs, NJ